



Contents lists available at ScienceDirect

Thin Solid Films

journal homepage: www.elsevier.com/locate/tsf

Raman spectra of *p*-type transparent semiconducting Cr₂O₃:Mg

Karsten Fleischer^{*}, David Caffrey, Leo Farrell, Emma Norton, Daragh Mullarkey, Elisabetta Arca, Igor V. Shvets

School of Physics and Centre for Research on Adaptive Nanostructures and Nanodevices (CRANN), Trinity College Dublin, Dublin 2, Ireland

ARTICLE INFO

Available online xxx

Keywords:

p-Type transparent conducting oxide
Raman spectroscopy
Dopant clustering
Cr₂O₃
Chromium sesquioxide

ABSTRACT

We present an analysis of the Raman spectra of *p*-type transparent conducting Cr₂O₃:Mg grown by various techniques including spray pyrolysis, pulsed laser deposition, molecular beam epitaxy and reactive magnetron sputtering. The best performing films show a distinct broad range Raman signature related to defect-induced vibrational modes not seen in stoichiometric, undoped material. Our comparative study demonstrates that Raman spectroscopy can quantify unwanted dopant clustering in the material at high Mg concentrations, while also being sensitive to the Mg incorporation site. By correlating the Raman signature to the electrical properties of the films, growth processes can be optimised to give the best conducting films and the local defect structure for effective *p*-type doping can be studied.

© 2015 Elsevier B.V. All rights reserved.

1. Introduction

p-Type transparent conductors are not only much sought after for the realisation of fully transparent CMOS type electronics [1], but also can play an important role in hole injecting or extracting layers for organic light emitting diodes or photovoltaic solar cells respectively [2–5]. In particular, oxide materials have been studied intensively since the first report of *p*-type transparent CuAlO₂ [6]. One of the better performing *p*-type transparent conducting oxides (TCOs) is CuCrO₂:Mg [7]. Despite its promising properties, the processing of this doped ternary oxide remains challenging and large variations in electrical properties depending on growth conditions have been reported [8]. Part of these problems is related to the dopant distribution and the other part is due to de-phasing of the ternary oxide itself [9–11]. Recently we have reported on a related doped binary oxide (Cr₂O₃:Mg and Cr₂O₃:Mg,N) with similar overall properties to CuCrO₂:Mg [12–14]. In contrast to CuCrO₂, Cr₂O₃ is the thermodynamically most stable chromium oxide, and hence the impact of the dopant distribution can be much easier studied.

In this paper we investigate the magnesium inclusion in this simpler binary system and will correlate how growth conditions influence the local micro-structure of the dopant measured by Raman spectroscopy. This is made possible by the rather simple Raman spectra of the binary oxide, allowing for a qualitative and quantitative analysis of defect induced vibrational modes introduced by the Mg dopant. We will show that electrical properties of Cr₂O₃:Mg are comparable between different growth techniques once the conditions are optimised to favour dissociation of dopant clusters during growth or post-annealing.

2. Experimental details

Thin film samples with a thickness between 100 and 300 nm have been grown on glass substrates or epitaxially on Al₂O₃(0001) by a variety of different techniques such as radio frequency (RF) magnetron sputtering, molecular beam epitaxy (MBE), spray pyrolysis (SP) and pulsed laser deposition (PLD).

RF sputtered samples have been prepared by co-sputtering from both a Cr metal target and an MgO ceramic target in a reactive plasma with Argon flow of 10 sccm with a substrate to target distance of 11 cm. The O₂ flow rate was raised to be the highest possible value (1.6 sccm) without system instability resulting from the formation of oxide on the metallic target surface (the oxide point). Alternatively, films have been prepared from sputtering in Ar only using a Cr₂O₃/MgO mixed target with nominal MgO weight content of 5%. Samples are typically grown at a pressure of 0.45 Pa and deposited onto a substrate heated to 950 K.

MBE grown samples have been prepared in a DCA M600 MBE with base pressure of 1.3×10^{-7} Pa at a substrate temperature of 875 K. Cr metal or ceramic Cr₂O₃ pieces were evaporated by e-beam heating with an oxygen partial pressure ranging from 1×10^{-4} to 5×10^{-3} Pa. The doping was achieved by controlling the supplied power to a second e-beam evaporator loaded with MgO. Details of the crystallographic and electrical properties of MBE grown films have been published elsewhere [14].

Details of the in-house built spray pyrolysis system and dependence of the Cr₂O₃:Mg properties on the precursor solution have been described in detail elsewhere [13]. For this study, the best performing films were grown using water based solutions of 0.1 M Cr(NO₃)₃ as a Cr precursor, 0.01 M MgCl₂·6(H₂O) as a cation dopant and 0.5 M NH₄CH₃CO₂ as an additive to improve film quality. Samples were sprayed using an air blast type nozzle operated with 120 kPa O₂, where substrates have been heated to 780 K.

^{*} Corresponding author.
E-mail address: fleisck@tcd.ie (K. Fleischer).

The PLD targets have been prepared in house by solid state reaction. Cr_2O_3 nano-powders and magnesium carbonate were mixed in a ratio of 94:6. In order to have a complete decomposition of the carbonate residual, leaving Mg as a dopant, powders were homogenised and then thermally treated at 1173 K for 24 h. Following this, the powders were grounded in a mortar with the addition of a few droplets of a solution of polyvinyl alcohol in isopropanol (15% w/w). This was necessary in order to preserve the integrity of the target during the following annealing steps. The powders were then pressed into pellets and sintered in air for at least 72 h at 1273 K. Samples were finally deposited from rotating targets at 773 K with a laser fluency of 0.3–0.5 J/cm², substrate to target distance of 7.5 cm, and oxygen back-pressure of 10 Pa.

For all samples the actual Mg content was measured by X-ray photoelectron spectroscopy (XPS) using Al $K\alpha$ photons in an Omicron Multiprobe XPS system. Surface contamination and residual precursor contamination was removed by Ar-sputtering at 650 V for 10–15 min with ion sputter currents of around 12.

The sheet resistance of all thin films was measured in linear four point probe geometry and the individual sample thickness has been determined by X-ray reflection, ellipsometry or cross sectional scanning electron microscopy depending on the thickness range or sample roughness. While the sheet resistance of the films varies with thickness, we will only discuss resistivity values $\rho = R_s d$, as they can be directly compared. All doped films show *p*-type conductivity as confirmed by Seebeck measurements.

Micro Raman spectra of all films have been taken with a Renishaw inVia Raman spectrometer in backscattering geometry using a 10 mW, 488 nm Argon–ion laser. For each sample polarisation dependent measurements were taken in $z(x, x)\bar{z}$ and $z(x, y)\bar{z}$ geometry. For the latter the scattered polarisation has been rotated by a $\lambda/2$ waveplate before the analysing polariser. This allows for direct intensity comparison of both spectra. To simplify the analysis only the Cr_2O_3 A_{1g} mode at 554 was analysed. Other modes as well the fluorescent background has been eliminated by subtracting the $z(x, x)\bar{z}$ and $z(x, y)\bar{z}$ signals. This way we only analyse the Raman signal in A_{1g} symmetry which removes substrate and E_g symmetry contributions from the spectra (see Fig. 1). All Raman spectra presented here are such differential data.

To compliment the crystallographic data from Raman spectroscopy, X-ray diffraction (XRD) patterns have been taken with a Bruker D8

Advance either in $\theta/2\theta$ geometry for epitaxial, or in grazing incidence geometry for thin, polycrystalline samples.

3. Results

With all investigated growth techniques we can synthesise Cr_2O_3 :Mg in the desired eskolaite phase and varying Mg concentration as confirmed by X-ray diffraction and XPS (not shown). For the investigated range of Mg doping all patterns are consistent with a single phase (eskolaite, Cr_2O_3 , PDF number 01-072-3533) [12,14]. As we investigated polycrystalline thin films grown on glass, as well as epitaxial films on Al_2O_3 , it is difficult to compare samples grown with different techniques based on their XRD pattern alone. Some exemplary patterns are shown in Fig. 2. In previous, more complete screening measurements the optimum Mg/Cr ratio for MBE and spray pyrolysis grown samples were found to be 8% or 10% respectively [13,14]. The resistivity of as grown films with Mg concentration of ~10% Mg/Cr ratio was found to be hugely dissimilar ranging from 1 to 5000 with PLD grown films showing lowest values and MBE and Magnetron grown samples from metallic sources showing the highest resistivity (see Table 1).

This initial result of widely varying resistivity values, despite samples showing similar crystal structure and dopant concentration, is quite similar to the situation reported for other oxide based *p*-type TCOs such as CuCrO_2 :Mg [8]. As previously discussed the phase diagram and Raman spectra of Cr_2O_3 are comparably simple. From a practical point of view we focus specifically on the strongest A_{1g} Raman mode using the polarisation dependent data. Vibrational modes in general are sensitive to the local bonding structure, and as doping levels are very high (>5%) we expect to see Mg related modes within the doped materials which will reflect the local coordination of the dopants. At high doping levels one could expect de-phasing of the material into other oxide phases such as stoichiometric Cr_2O_3 , MgCr_2O_4 , or MgO. We therefore first investigated the Raman signature as a function of Magnesium concentration for magnetron sputtered samples, as this technique offered the easiest and most robust control of Mg/Cr ratio via the applied power to the Cr and MgO target. Fig. 3 shows the development of a Mg related local vibrational mode (LVM) around 720 already for low Mg concentrations. The broad structure in the vicinity of

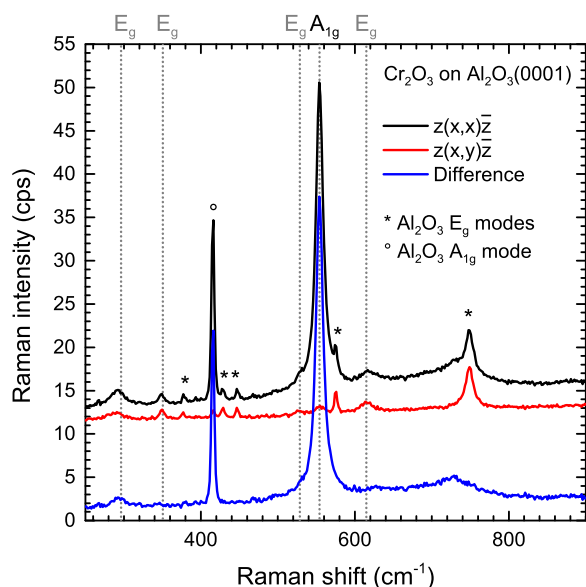


Fig. 1. Raman spectra of an undoped, stoichiometric Cr_2O_3 thin film on $\text{Al}_2\text{O}_3(0001)$ in two different scattering geometries and the difference between them resulting in an A_{1g} symmetry only signal. This data analysis allows for a better peak shape analysis of the Cr_2O_3 A_{1g} mode at 554 as overlapping Cr_2O_3 and substrate E_g modes are removed.

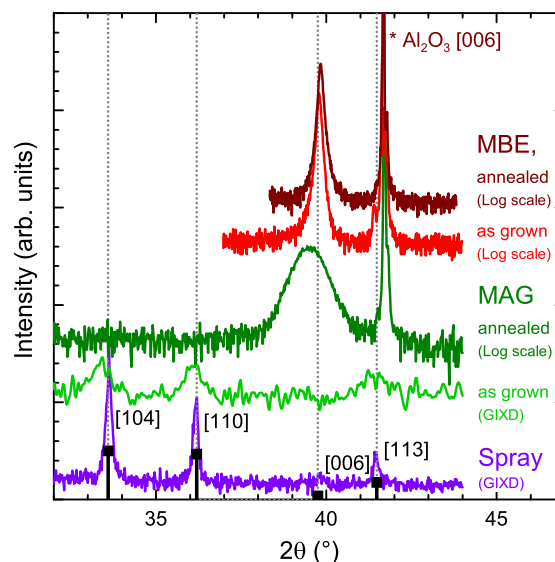


Fig. 2. XRD patterns of selected as grown and post-annealed Cr_2O_3 :Mg samples grown with various techniques. All films show only peaks consistent with the eskolaite phase, with small differences in peak width, *a* – and *c* – lattice parameter. These are caused by differences in oxygen stoichiometry, crystalline quality, and film thickness. All samples shown had doping levels of $10 \pm 2\%$. Polycrystalline samples grown on glass have been measured in grazing incidence geometry, samples grown on sapphire in $\theta/2\theta$ geometry and shown in logarithmic scale for better comparison.

Table 1

Comparison of representative samples in terms of their resistivity. Critical growth parameters including oxygen partial pressure (p_{O_2}), temperature T have been given for samples grown by different techniques (MBE, PLD, Spray Pyrolysis (SPR), and Magnetron sputtering (MAG)). The actual Mg content for each sample, as well as measured resistivity ρ , frequency $\omega_{A_{1g}}$ and width Γ of the main $Cr_2O_3 A_{1g}$ mode have also been listed. Samples shown in Fig. 6 are indicated.

Sample	Cr source	p_{O_2} (Pa)	T (K)	Mg/Cr (%)	Comment	Substrate	ρ (Ω cm)	$\omega_{A_{1g}}$ (cm^{-1})	Γ (cm^{-1})
<i>Initial growth mode</i>									
MBE-13A	Metal	1.4×10^{-3}	875	10	As grown	Al_2O_3	60	546	14
MBE-13B	Metal	1.4×10^{-3}	875	10	Post-annealed	Al_2O_3	25	546	14
MBE-39A	Oxide	1.4×10^{-3}	875	8	As grown	Al_2O_3	20	–	–
MAG-55A	Metal	6.5×10^{-2}	975	9	As grown	Glass	5000	548	17
MAG-139	Oxide	9×10^{-2}	97	5	As grown, F6	Glass	80	556	37
MAG-181A	Metal	9×10^{-2}	1085	13	As grown	Al_2O_3	64	550	29
PLD-88A	Oxide	10	775	8	As grown, F6	Al_2O_3	1	553	16
SPR-26A	Nitrate	1×10^5	800	10	As grown, F6	Glass	4	534	31
<i>After change in growth procedure for MBE and RF sputtering</i>									
MBE-39B	Oxide	4×10^{-3}	875	8	Post-annealed, F6	Al_2O_3	5.5	552	17
MAG-181B	Metal	9×10^{-2}	1085	13	Post-annealed, F6	Al_2O_3	2	554	25

the $Cr_2O_3 A_{1g}$ mode seen already for undoped samples is caused by the glass substrate. The LVM is well developed and not as broad as expected for localised defect centres, suggesting a de-phasing of the material on the nanometre range as X-ray diffraction patterns did not reveal other phases rather than the eskolaite Cr_2O_3 phase. One likely candidate of a phase separation would be the $MgCr_2O_4$ spinel structure. Its main A_{1g} mode in bulk form however is found at 685. In strain dependent Raman measurements however it was shown that the $MgCr_2O_4$ mode shifts significantly to higher frequencies under uniaxial strain [15]. To observe the mode at 720 strain values of 15 GPa would be required. Such values are not unreasonable for nanometre sized clusters embedded in a Cr_2O_3 matrix, hence, our data is consistent with the formation of dopant clusters in the form of $MgCr_2O_4$ inclusions, which explain the poor electrical properties of these as grown samples.

In a second step the Raman spectra of MBE grown samples grown on $Al_2O_3(0001)$ have been analysed. The thin films are fully relaxed with improved conductivity compared with the polycrystalline films grown on glass by RF-sputtering, but still far from the ideal 1–5 seen in PLD and SP grown films. As grown samples, using Cr metal and MgO as

dopant, show a combination of a broad defect induced mode around 620 and a similar mode at 720 (see Fig. 4). The latter mode is significantly reduced once samples are post-annealed in oxygen, while at the same time the Cr_2O_3 mode is sharpened, the broad defect mode increased and the conductivity of the thin film improved. This can be interpreted as a direct redistribution of the Mg in the film from localised, strained $MgCr_2O_4$ clusters to more isolated defects required for cationic doping.

For all these samples the position of the $Cr_2O_3 A_{1g}$ was found to be below the expected bulk value of 554. This difference could be related to Mg induced strain however the position did not significantly vary with increased Mg concentration or Mg redistribution during post-annealing. As all samples so far have been grown from metallic targets at the highest oxygen partial pressure available in the instrument, the change could be caused by a lack of oxygen in the lattice. p -Type oxides are typically improved with high oxygen partial pressure. Hence, another set of samples have been prepared by using Cr_2O_3 pellets as source material for e-beam evaporation. Fig. 5 shows the Raman spectra of

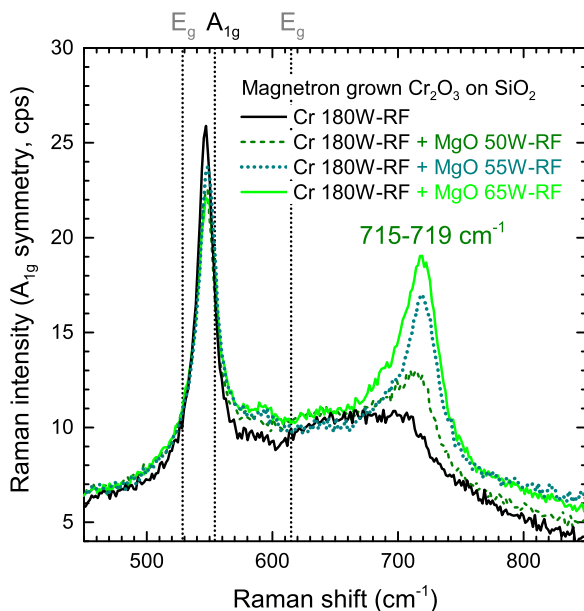


Fig. 3. Differential Raman signal (A_{1g} symmetry) for Cr_2O_3 as a function of power to the MgO target. Samples were grown on glass, which adds a broad, Raman background as already seen in the plain Cr_2O_3 spectra. With increasing Mg incorporation a pronounced local vibrational mode appears around 720, accompanied with a broadening and intensity reduction of the $Cr_2O_3 A_{1g}$ mode.

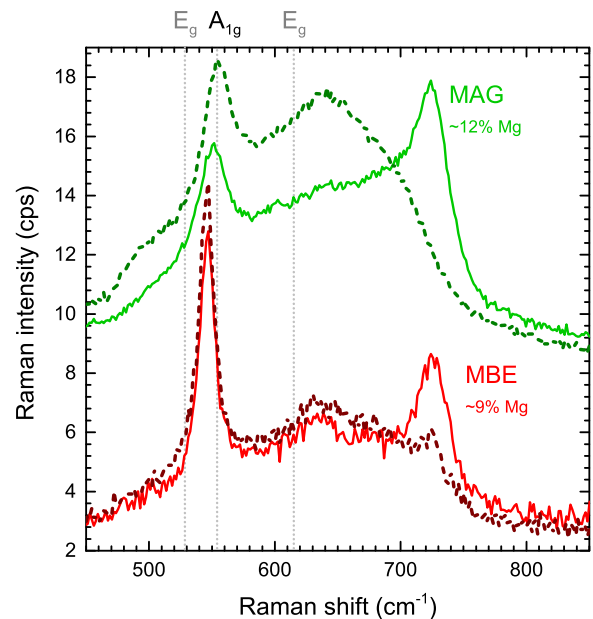


Fig. 4. Differential Raman signal (A_{1g} symmetry) for $Cr_2O_3:Mg$ as grown by MBE. The sample had a Mg/Cr ratio of 9% as measured by XPS and the resistivity dropped from 60 to 24 during the post-annealing in oxygen at 700 (dashed, red line). This is accompanied with a significant reduction of the LVM linked to the presence of $MgCr_2O_4$ clusters. The second set demonstrates the same effect of post-annealing in a magnetron grown sample with considerably higher Mg concentration (~12%). In the latter case the improvement in resistivity is even more pronounced 64 to 2 Ω cm.

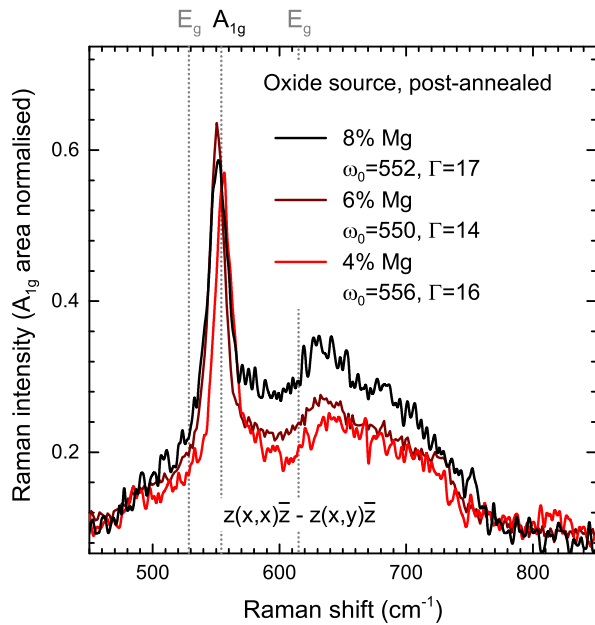


Fig. 5. Differential Raman signal (A_{1g} symmetry) for $\text{Cr}_2\text{O}_3:\text{Mg}$ as grown by MBE from ceramic oxide pellets as a function of Mg concentration. In this case, the $\text{Cr}_2\text{O}_3 A_{1g}$ is found closer to the expected bulk value.

these films as a function of Mg concentration and after the usual post-annealing step. The unwanted MgCr_2O_4 related mode is not seen anymore in favour of the Mg defect related broad band mode. Consequently the resistivity of the sample with ideal Mg concentration was found to be in line with best performing SP grown films at 5.

Similar improvements have been observed for RF sputtered films once the metallic target was changed to a ceramic one. The latter $\text{Cr}_2\text{O}_3:\text{MgO}$ mixed target had a nominal Mg/Cr atomic ratio of 5%, and further improvements are expected once this is increased to values of around 10%. Once the target composition, growth and post-annealing conditions have been optimised to maximise the oxygen partial pressure, the formation of MgCr_2O_4 clusters in the thin films is suppressed, either due to an increased formation energy of MgCr_2O_4 , or the decrease in formation energy for the active doping defect, most likely Mg_{Cr} . These findings are very similar to early reports on the solubility of MgO in Cr_2O_3 in solid solutions formed at high temperatures, where an increase in oxygen pressure was found to increase solubility [16].

When this is combined with post-annealing to dissociate any residual clusters the spread in electrical performance of films prepared by different techniques was reduced from three orders of magnitude to below one (see Table 1). In this case, all films show a broad band defect related mode around 620 in the Raman spectra in addition to the main $\text{Cr}_2\text{O}_3 A_{1g}$ mode. Fig. 6 shows Raman spectra of samples grown with various techniques. There are still differences in crystallinity as indicated by a considerable difference in broadening and position of the $\text{Cr}_2\text{O}_3 A_{1g}$ mode particularly for non epitaxial films. Further studies are required to correlate these changes to differences in crystal orientation, size, oxygen stoichiometry, and their influence on the electrical properties of the material. Most importantly, none of these optimised samples shows the signature associated with unwanted dopant clustering.

4. Conclusion

We have demonstrated that large differences in resistivity between $\text{Cr}_2\text{O}_3:\text{Mg}$ samples are related to a clustering of the Mg precursor. Depending on growth conditions the dopant clusters into regions which are too small to be detectable by XRD, but large enough to result in a coherent local vibrational mode seen in Raman spectroscopy. The most likely structure of these clusters is highly strained MgCr_2O_4 . By

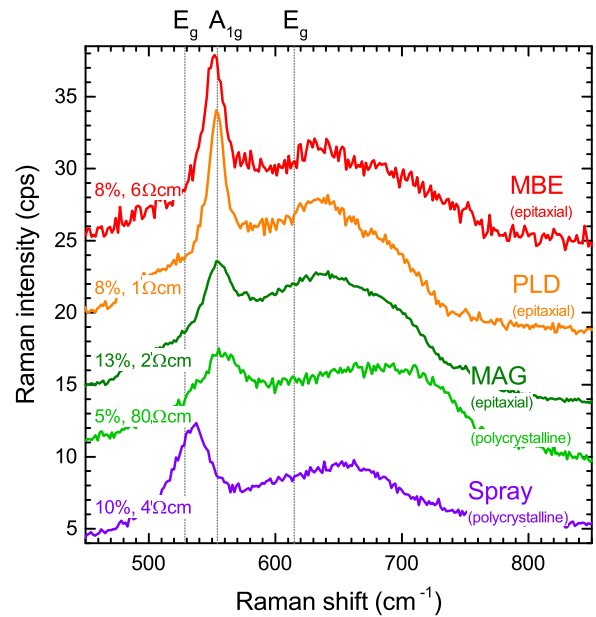


Fig. 6. Differential Raman signal (A_{1g} symmetry) for $\text{Cr}_2\text{O}_3:\text{Mg}$ grown by various techniques on Al_2O_3 (MBE, PLD, MAG) or glass (MAG, SP) and conditions maximising the oxygen partial pressure by using ceramic targets, or using postannealing (MAG, epitaxial). No samples show the LVM at 720.

post-annealing these clusters can be partially dissociated and under optimum growth conditions using ceramic targets and high oxygen partial pressure the occurrence of this phase can be fully suppressed. This assessment is based on the changes in Raman spectra of the thin films, using particular differential measurements that dominantly show A_{1g} symmetry Raman modes.

While these studies are based on $\text{Cr}_2\text{O}_3:\text{Mg}$ we believe that findings are more general and results can be applicable to other Mg doped oxide semiconductors in particular $\text{CuCr}_2\text{O}_2:\text{Mg}$, where a similar formation of unwanted spinel phase has been reported [10]. The physical mechanisms of suppressing this localised dopant clustering during growth or post-growth by annealing in oxygen are likely very similar in Cr_2O_3 and CuCr_2O_2 .

Acknowledgements

The authors would like to thank Science Foundation Ireland under grant no. 12/IA/1264, the Irish Research Council under grant numbers GOI/PG/2013/445 and GOI/PG/2013/444, and the Higher Education Authority under the PRTL scheme, cycle 5 for their financial support.

References

- [1] A. Facchinetti, T.J. Marks, *Transparent Electronics From Synthesis to Application*, Wiley, 2010.
- [2] J. Meyer, S. Hamwi, M. Kroger, W. Kowalsky, T. Riedl, A. Kahn, *Transition metal oxides for organic electronics: energetics, device physics and applications*, *Adv. Mater.* 24 (40) (2012) 5408.
- [3] Q.H. Wu, *Progress in modification of indium-tin oxide/organic interfaces for organic light-emitting diodes*, *Crit. Rev. Solid State Mater. Sci.* 38 (4) (2013) 318.
- [4] S. Chen, J.R. Manders, S.W. Tsang, F. So, *Metal oxides for interface engineering in polymer solar cells*, *J. Mater. Chem.* 22 (46) (2012) 24202.
- [5] J. Bandara, J.P. Yasomane, *P-type oxide semiconductors as hole collectors in dye-sensitized solid-state solar cells*, *Semicond. Sci. Technol.* 22 (2) (2007) 20.
- [6] H. Kawazoe, M. Yasukawa, H. Hyodo, M. Kurita, H. Yanagi, H. Hosono, *P-type electrical conduction in transparent thin films of Cu_2O* , *Nature* 389 (6654) (1997) 939.
- [7] R. Nagarajan, N. Duan, M.K. Jayaraj, J. Li, K.A. Vanaja, A. Yokochi, A. Draeseke, J. Tate, A.W. Sleight, *p-Type conductivity in the delafossite structure*, *Int. J. Inorg. Mater.* 3 (3) (2001) 265.
- [8] A. Stadler, *Transparent conducting oxides—an up-to-date overview*, *Materials* 5 (4) (2012) 661.
- [9] D.O. Scanlon, G.W. Watson, *Understanding the p-type defect chemistry of CuCr_2O_2* , *J. Mater. Chem.* 21 (11) (2011) 3655.

- [10] R. Bywalez, S. Goetzdoerfer, P. Loebmann, Structural and physical effects of Mg-doping on p-type CuCrO_2 and $\text{CuAl}_{0.5}\text{Cr}_{0.5}\text{O}_2$ thin films, *J. Mater. Chem.* 20 (31) (2010) 6562.
- [11] J. Robertson, R. Gillen, S. Clark, Advances in understanding of transparent conducting oxides, *Thin Solid Films* 520 (10) (2012) 3714.
- [12] E. Arca, K. Fleischer, I. Shvets, Magnesium, nitrogen codoped Cr_2O_3 : a p-type transparent conducting oxide, *Appl. Phys. Lett.* 99 (11) (2011) 111910.
- [13] E. Arca, K. Fleischer, S. Krasnikov, I. Shvets, Effect of the chemical precursors on the optical and electrical properties of p-type transparent conducting Cr_2O_3 :(Mg, N), *J. Phys. Chem. C* 117 (2013) 21901.
- [14] L. Farrell, K. Fleischer, D. Caffrey, D. Mullarkey, E. Norton, I.V. Shvets, Conducting mechanism in the epitaxial p-type transparent conducting oxide Cr_2O_3 :Mg, *Phys. Rev. B* 91 (12) (2015) 125202 (URL <http://link.aps.org/doi/10.1103/PhysRevB.91.125202>).
- [15] Z. Wang, H. O'Neill, P. Lazor, S. Saxena, High pressure Raman spectroscopic study of spinel MgCr_2O_4 , *J. Phys. Chem. Solids* 63 (11) (2002) 2057.
- [16] M.Y. Su, G. Gimkovich, Point defect structure of Cr_2O_3 , Tech. Rep. TR 87-008, The Pennsylvania State University, 1987.